Porous Layered Double Hydroxide/TiO2 Photocatalysts for the Photocatalytic Degradation of Orange II

Rodrigue Djeda, Gilles Mailhot, Vanessa Prevot

chemengineering

MDPI

Article

Porous Layered Double Hydroxide/TiO_2 Photocatalysts for the Photocatalytic Degradation of Orange II

Rodrigue Djeda [1,*], Gilles Mailhot [2] and Vanessa Prevot [2,*]

[1] UFR Environnement, Département de Chimie Informatique Mathématiques et Physique, Université Jean Lorougnon Guédé, BP 150 Daloa, Cote d'Ivoire

[2] Institut de chimie de Clermont-Ferrand (ICCF), Université Clermont Auvergne, CNRS, Sigma Clermont, F-63000 Clermont-Ferrand, France; gilles.mailhot@uca.fr

* Correspondence: rodrigue.djeda@gmail.com (R.D.); vanessa.prevot@uca.fr (V.P.); Tel.: +22504345152 (R.D.); +33473405167 (V.P.)

Received: 27 April 2020; Accepted: 8 June 2020; Published: 10 June 2020

Abstract: Layered Double Hydroxide (LDH)/TiO_2 nanocomposites with photocatalytic properties were synthesized by both impregnation and the direct coprecipitation of LDH matrices using a colloidal suspension of TiO_2 nanoparticles. While the two methods led to an efficient TiO_2 nanoparticle immobilization, the direct coprecipitation allowed us to tune the amount of immobilized TiO_2 within the materials. The LDH/TiO_2 nanocomposites obtained were deeply characterized by chemical analysis (ICP-AES), Powder X-ray diffraction (XRD), Fourier Transformed Infra-Red (FTIR), Thermogravimetric analysis (TGA), and High-Resolution Transmission Electron Microscopy (HRTEM). Clearly, the immobilization of TiO_2 by direct coprecipitation promoted a modification of the textural properties and a net increase in the surface area. The crystallized TiO_2 nanoparticles can be distinctly visualized by HRTEM at the surface of the layered material. Several parameters, such as the nature of the chemical composition of LDH (ZnAl and MgAl), the method of immobilization and the amount of TiO_2, were shown to play a crucial role in the physicochemical and photocatalytic properties of the nanocomposites. The photocatalytic efficiency of the different LDH/TiO_2 nanocomposites was investigated using the photodegradation of a model pollutant, the Orange II (OII), and was compared to a pure TiO_2 colloidal solution. The degradation tests revealed that the nanocomposite obtained from MgAl LDH at a low MgAl LDH/TiO_2 ratio was the most efficient for the photodegradation of OII leading to complete mineralization in 48 h.

Keywords: photodegradation; titanium dioxide; LDH; Orange II; nanocomposites; coprecipitation; impregnation

1. Introduction

Dyes, as all other organic compounds, are introduced into water bodies through waste from industrial processes such as pharmaceutical, dyes and textiles, petrochemicals, and pesticide factories [1,2]. The presence of these compounds in water bodies, such as rivers, lakes, and oceans, results in huge environmental pollution by industrial waste. Water bodies polluted by toxic and carcinogenic organic compounds pose a threat to aquatic organisms, plants, animals, and humans [3–6]. Besides, the accumulation of these dyes in aquatic species can lead to animal and human toxicity through the food chain [7,8]. In some cases, with these non-biodegradable and often highly oxidizable compounds, the pH of the medium may decrease and thus cause a considerable increase in toxicity for the ecosystems. For the organisms living in an aquatic medium, animals are more sensitive to toxicity than plants. Often, even at very low concentrations, the specific odors of these chemical pollutants are emitted into the water and even contaminate the flesh of fish [9,10]. These polluted waters can, in turn, contaminate the groundwater reserve of natural drinking

water for human consumption. To address this rigorously, the need for sewage treatment is needed by humanity [11,12], although, in most cases, the pollutants are in a diluted state in the waters, which is sufficient for toxicity [13].

TiO_2 nanoparticles are currently widely studied as a photocatalyst for renewable energy production and water treatment [14,15]. Thus, many groups of researchers have studied and are still studying the degradation of different pollutants by this process, as well as the factors influencing its effectiveness and the elementary mechanism of the formation of active species in this system. TiO_2 exists mainly in three crystalline forms—anatase, rutile, and brookite—but there are other synthetic forms obtained under high pressure. In the presence of moisture, the surface of the pure titanium dioxide is covered by hydroxyl groups [16,17]. Anatase is considered a more effective crystalline form than rutile for the photocatalytic degradation of most pollutants [18–20]. The species responsible for the pollutant photodegradation using TiO_2 is the hydroxyl radical $^{\bullet}OH$, a highly reactive species that can induce the oxidation of all organic molecules. The photocatalytic process depends on the release of e_{CB}^- electrons promoted from the valence band (VB) to the conduction band (CB), leaving a positive hole h_{VB}^+. This hole h_{VB}^+ directly oxidizes organic matter or reacts with an electron-donating species, such as water forming free radicals $^{\bullet}OH$. These free radicals react with organic compounds as dyes, chlorophenols, and other compounds [21]. In addition, the promoted electron e_{CB}^- can react with O_2 to form a superoxide anion radical ($O_2^{\bullet -}$) [22,23].

To improve the efficiency and applicability of TiO_2, several strategies to reduce the band gap, limit the electron-hole recombination, and to enhance the pollutant adsorption were investigated, involving doping, sensitization, oxygen defects, nanostructuration, and their associations with other materials [24]. In the field of environmental clean-up, the photocatalytic efficiency of supported TiO_2 is promising, but in some cases, the fixation method limits the efficiency and consumes excessive energy because of the high temperature [25]. TiO_2 nanoparticles were immobilized on glass plates using heat fixation methods, resulting in photocatalyst plates that could be used for dye degradation [26]. According to other approaches, the use of bonding materials, such as polysiloxane, were used for fixing photocatalysts for repetitive use [27]. The sol-gel approach was also tested for TiO_2 film preparation in parallel to pulsed laser deposition, liquid phase evaporation anodization, or chemical vapor deposition [27–29]. Interestingly, it was demonstrated that, for mesoporous nanocrystalline anatase, the photocatalytic efficiency depended on the pore network [30–32].

Moreover, various materials were tested as immobilization supports for TiO_2 nanoparticles, such as magnetic particles to improve their recovery from the solution using a magnetic field [33]. Amongst the different materials used in combination with TiO_2, layered double hydroxides (LDH) have gained increasing attention. LDH possess a brucite-like layered structure in which a part of divalent metal cations is substituted by trivalent one. The positive charge generated at the layer surface is balanced by the presence of intercalated anions in between the layers [34,35]. These matrices are known for their adsorbent properties, allowing for the adsorption of organic compounds causing pollution [36]. In addition to the high adsorption capacity of LDH, the cost of the raw material is affordable and its preparation is easy to carry out. LDH are valuable adsorbents of interest for the removal of pollutants, such as anionic dyes like orange II [37–39]. The removal of dyes by adsorption is less expensive than other methods, easy to handle, and maintenance costs less. In the literature, various photocatalysts based on LDH containing titanium or in association with TiO_2 and their derived mixed metal oxides, have been described for their applications in the field of solar cells, water splitting, CO_2 photoconversion, sunscreen, supercapacitors and antimicrobial materials [40–48]. LDH/TiO_2 assemblies have also been investigated for their efficiency toward pollutant photodegradation [49–51]. In this approach, LDH is mainly expected to: (1) enhance the vicinity of the organic pollutant with the TiO_2 surface, thanks to the LDH adsorption properties; (2) facilitate the photocatalyst's recovery by filtration; (3) limit the TiO_2 nanoparticle aggregation through a homogeneous distribution on the two-dimensional materials.

In this work, different approaches were investigated to synthesize porous TiO_2@LDH photocatalytic nanocomposites, in which the immobilized TiO_2 photocatalytic properties are combined with the LDH adsorption, with the aim of establishing contact between the reactive sites (h_{VB}^+; e_{CB}^-) and pollutant required in addition to $^{\bullet}OH$ and other reactive species. The effect of the TiO_2 immobilization technique, the LDH chemical composition, and TiO_2 aging on the nanocomposite properties were studied in detail with the aim of shedding light on the relationship between the material properties and the photocatalytic efficiency recorded.

2. Materials and Methods

2.1. Materials Preparation

Orange II ≥ 85% (OII); $HClO_4$ 70%; KNO_3 99%, Na_2CO_3 99%, and NaOH 97% were purchased from Merck. KOH; $Zn(NO_3)_2{\cdot}6\,H_2O$ 98%; $Mg(NO_3)_2{\cdot}6\,H_2O$ 98%; $Al(NO_3)_3{\cdot}9H_2O$ 98%, $AlCl_3{\cdot}6H_2O$ 98%, HNO_3, and $TiCl_4$ 99% were purchased from Acros Organics or Sigma-Aldrich. These products have been used without further purification. Deionized water obtained from a water purification system showing resistivity of 18.0 MΩ cm was systematically used with no additional degassing step. N_2 gas (99%) was used without further drying or deoxygenation as a protective atmosphere.

To prepare colloidal TiO_2 nanoparticles, 3.5 mL of pure $TiCl_4$ was added dropwise into 900 mL of deionized water, stirred vigorously and cooled to 1 °C as previously reported [52]. The solution was then further stirred for 30 min and finally dialyzed with Spectrapor membrane up to pH = 2.50. When necessary, deionized water was added to obtain a total volume of the solution of 960 mL, which corresponds to a concentration of Q-TiO_2 equal to 33.3 mM (2.66 g L^{-1}). The granulometric analysis by dynamic light scattering reveals that synthesized Q-TiO2 particles were of 5 nm in diameter, as shown in Figure 1B. Aged TiO_2 was obtained by letting the colloidal solution for three months at 4 °C. Prior to the immobilization step, a basic colloidal dispersion of TiO_2 was prepared by quickly adding a 2 M KOH solution to the acidic colloidal TiO_2 solution under ultrasound. The clear dispersion thus obtained has a pH = 9.30.

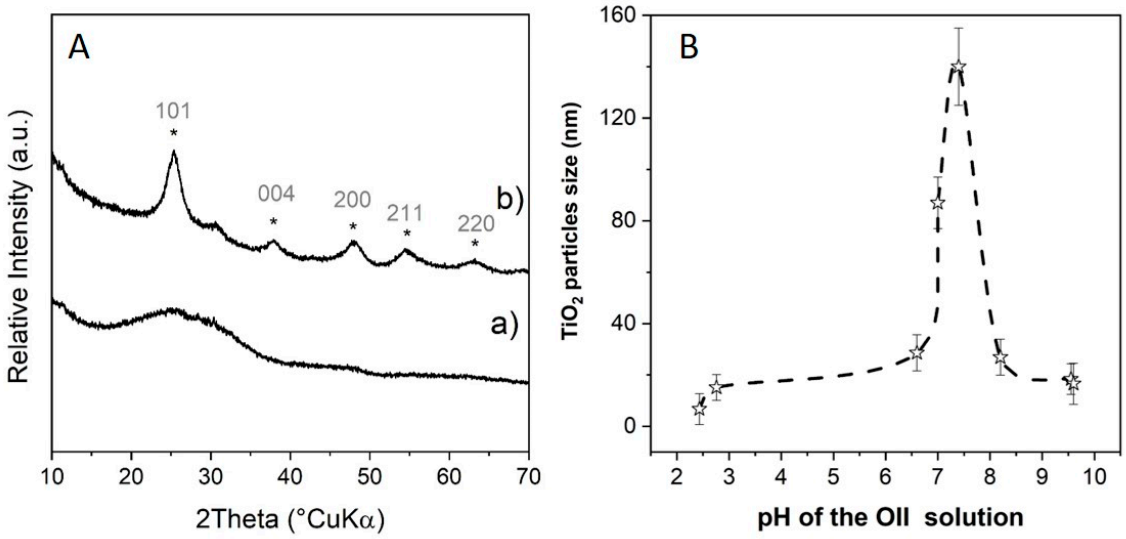

Figure 1. (**A**) PXRD of (**a**) colloidal TiO_2 freshly prepared, (**b**) colloidal TiO_2 after three months of storage at 4 °C. (**B**) Evolution of the TiO_2 particle size during titration with concentrated KOH.

[Zn_2Al] and [Mg_2Al] phases were synthesized by coprecipitation at constant pH = 8.00 and pH = 10.00, respectively [34]. Typically, a 0.2 M metal salt aqueous solution (M^{II}/M^{III} = 2) was slowly added in a reactor containing either potassium nitrate (1 M) or sodium carbonate (0.5 M), according to the anion to be intercalated. For the nitrate intercalated LDH, a protective N_2 atmosphere was used. The pH of the reaction medium was kept constant by the controlled addition of a 2 M

sodium hydroxide solution. After addition, the reaction medium was stirred for 24 h. The solid was then collected by centrifugation and subjected to three wash cycles. For the [Zn_2Al-NO_3] sample used for TiO_2 immobilization by impregnation, one part was dried overnight at room temperature to get LDH powder (noted dry), while another part was kept dispersed in an aqueous solution to avoid the irreversible aggregation of the particles during the drying step (noted wet).

TiO_2 colloidal particles were immobilized by impregnation on [Zn_2AlNO_3] by adding a suspension of 100 mL of colloidal TiO_2 (0.5 g L^{-1}) in a reactor containing 0.1 g of LDH, which corresponds to a mass ratio of LDH/TiO_2 = 2. The solution was subjected to mechanical stirring for approximately 20 h under a protective N_2 atmosphere. The LDH precursors used were either in the form of dried powder or wet suspension and the resulting samples are hereafter noted $[Zn_2Al/TiO_2]_{dry}$ and $[Zn_2Al/TiO_2]_{wet}$.

In an alternative strategy, TiO_2 colloidal particles were also directly immobilized during LDH coprecipitation. A similar procedure as previously described for the LDH synthesis was performed except that a basic colloidal solution of TiO_2 was initially introduced into the reactor. Typically, a fixed volume of 0.2 M metal salt solution was added simultaneously with 2 M NaOH/0.5 M Na_2CO_3 to the reactor containing TiO_2, to maintain the pH at 9.30 and 10.00 for [Zn_2Al/TiO_2] and [Mg_2Al/TiO_2], respectively. The theoretical LDH/TiO_2 ratios were fixed by controlling the volume of basic colloidal TiO_2 added ([TiO_2] = 2.66 g L^{-1}), the metal salt volume being maintained constant. The [Zn_2Al/TiO_2] coprecipitated sample was prepared for an LDH/TiO_2 ratio of 2 while four [Mg_2Al/TiO_2] samples were prepared for ratios of 8, 4, 2, and 0.66. After the addition, the reaction medium was stirred for 24 h. The solid was then collected by centrifugation and subjected to three washing cycles and dried at room temperature.

2.2. Characterization

The sizes of the TiO_2 particles were measured by dynamic light scattering (DLS). These measurements were carried out on a Zetasizer Nanoseries (Malvern Instrument) on very dilute dispersion. Zeta potential (ξ) was also determined using the same equipment. The errors were estimated based on the standard deviation of three measurements and a reproducibility test. All X-ray diffraction measurements were made on a X-PERT PRO PHILIPS powder diffractometer equipped with X-Celerator detector. The diffractograms were carried out under the following operating conditions: angular domain 2θ (5°–70°), angular increment 2θ (0.0836°), and counting integration time (130.17 s). The infrared spectroscopy measurements were obtained using a NICOLET 5700 Fourier Transform spectrometer. The measurements were carried out in attenuated total reflection (ATR). The spectra were acquired in absorbance for wavenumbers between 4000 and 400 cm^{-1}, a resolution of 8 cm^{-1}, and a number of 32 scans. The chemical compositions of the samples were determined by inductively coupled plasma atomic emission spectroscopy (ICP-AES) on a HORIBA-Jobin-Yvon ULTIMA C spectrometer. Analyses by high-resolution transmission electron microscopy (HRTEM) were carried out on a JEOL JEM 3010 microscope (200 kV, LaB6cathode) equipped with a CCD camera. The samples were dispersed in ethanol and further treated in ultrasound for 20 min. In order to carry out the analyses, a drop of the dilute suspension was placed on a holey-carbon-coated copper grid and was left to dry at room temperature. The Energy Dispersive X-ray (EDX) spectra were collected from several locations. Nitrogen adsorption–desorption experiments were performed at −196 °C with a Micromeritics ASAP 2020. The samples were pretreated at 80 °C under vacuum for 12 h. The surface areas were calculated using the Brunauer–Emmett–Teller method. Thermogravimetric analyses (TGA) were recorded on a Setaram TG-DTA 92 instrument in the temperature range of 25–1000 °C, with a heating rate of 5 °C min^{-1}. The measurement of the total organic carbon concentration to follow the mineralization of OII was monitored using a TOC-5050 Analyzer (Shimadzu).

2.3. Photocatalytic Activity

The irradiation was performed in a setup with three medium-pressure mercury vapor lamps (MAZDA HPW 125W) whose emission, filtered by a black globe, was mainly at 365 nm (93% light).

A water-jacketed Pyrex tube centered into the setup was used as a reactor. The amount of photocatalyst involved in the photodegradation experiment was systematically calculated to correspond to [TiO_2] = 0.5 g L^{-1}. The concentration of OII used as a model pollutant was fixed at 5.10^{-5} M and the solution was continuously stirred during the experiment. The amount of OII in the solution was determined at different intervals of time by UV–vis spectroscopy using a Varian Cary 100 Scanning UV–vis spectrophotometer, by monitoring the absorbance at λ_{max} = 484 nm and by using the Beer–Lambert law. Being an anionic dye, OII strongly adsorbs on LDH, as shown in Supplementary Materials, Figure S1. To discriminate between adsorption and photodegradation, the LDH matrices were dissolved before OII dosage by adding an acidic solution (HCl 1 M) until pH = 3.0, to induce the release of the OII adsorbed on the LDH in solution. The calibration curve and the "apparent" absorption coefficients were established in these conditions. Photodegradation experiments, involving [Zn_2Al-NO_3] and [Mg_2Al-CO_3] LDH precursors without TiO_2, were performed to confirm that, in these conditions, the amount of OII photodegraded was negligible.

3. Results and Discussion

3.1. TiO_2 Colloidal Dispersion

Granulometric analysis of the colloidal dispersion of TiO_2 at pH 2.50 revealed that the particle size was 5 nm after synthesis, as shown in Figure 1B. A limited size increase was observed after three months of aging at 4 °C, with a particle size centered at 11 nm and a ξ of +39 mV, as previously reported [52]. However, such aging was accompanied by the enhancement of the crystallinity of the particles, evidenced on the PXRD displaying reflection lines typical of the anatase phase, as shown in Figure 1A. The width of the reflections was in good agreement with very small coherent domain sizes. To promote the use of colloidal TiO_2 for environmental applications in neutral or basic pH and to make the surface charge of the nanoparticles compatible with the LDH, a titration was carried out using concentrated KOH solution. Titanium oxides are known to be amphoteric in aqueous suspensions. The equilibrium constants determined for Degussa P25 TiO_2 are pK_{a1} = 4.50 and pK_{a2} = 8.00 [53]. These results lead to the value of the zero-charge point pH_{ZPC} = 6.25. In good agreement, the studied TiO_2 colloidal suspension coagulates for intermediate pH values in the range 6–8 due to the neutralization of the surface charge, leading to aggregation, as shown in Figure 1B. At pH higher than 9, the charge inversion proceeded and the change in particle size was limited. A clear basic colloidal dispersion of TiO_2 was obtained at 9.30 with a particle size centered at 15 nm (ξ = −41 mV) in good agreement with TEM image, as shown in Supplementary Materials, Figure S2. As a result, in the following parts, the TiO_2 dispersion at pH 9.30 was used for the synthesis of LDH/TiO_2 assemblies.

3.2. LDH/TiO_2 Nanocomposite Preparation and Characterization

Various [LDH/TiO_2] composites were prepared to evaluate the influence of parameters such as the immobilization method, the LDH chemical composition, and the TiO_2 physico-chemical properties in the photocatalyst efficiency of OII degradation.

Two different strategies were tested to prepare the LDH/TiO_2 nanocomposites: the impregnation and the direct coprecipitation. The impregnation process is based on a simple contact in solution under stirring between an LDH precursor phase and colloidal TiO_2 nanoparticles. At basic pH, the TiO_2 immobilization is promoted by electrostatic interaction between LDH layers and TiO_2 nanoparticles. In a preliminary step, a [Zn_2Al-NO_3] LDH phase was prepared by classical coprecipitation. The PXRD pattern displays the main characteristic reflections expected for a pure LDH phase in a rhombohedral R-3m structure, especially with the 003, 006, 120, 110 and 113, *as shwon in* Figure 2*A*. The position of the 00l reflection lines indicated an interlamellar distance equal to 0.83 nm, confirming the formation of nitrate intercalated LDH. The presence of nitrate as interlayer anion is further confirmed by FTIR and the presence of an intense band at 1403 cm^{-1}, as shown in Figure 2B. The band observed at 1357 cm^{-1} could indicate partial contamination by carbonate anions adsorbed at the LDH particle

surface. The other bands observed were characteristic of the LDH matrices with the vibrations of the OH groups at 3400–3600 cm^{-1}, the vibrations of the H_2O molecules in the interlayer at 3100–3200 cm^{-1} for the OH valencies, and 1650 cm^{-1} for the deformation vibrations. The bands below 850 cm^{-1} were attributed to the vibrations of the M-O and the deformation of the M-O-M bonds.

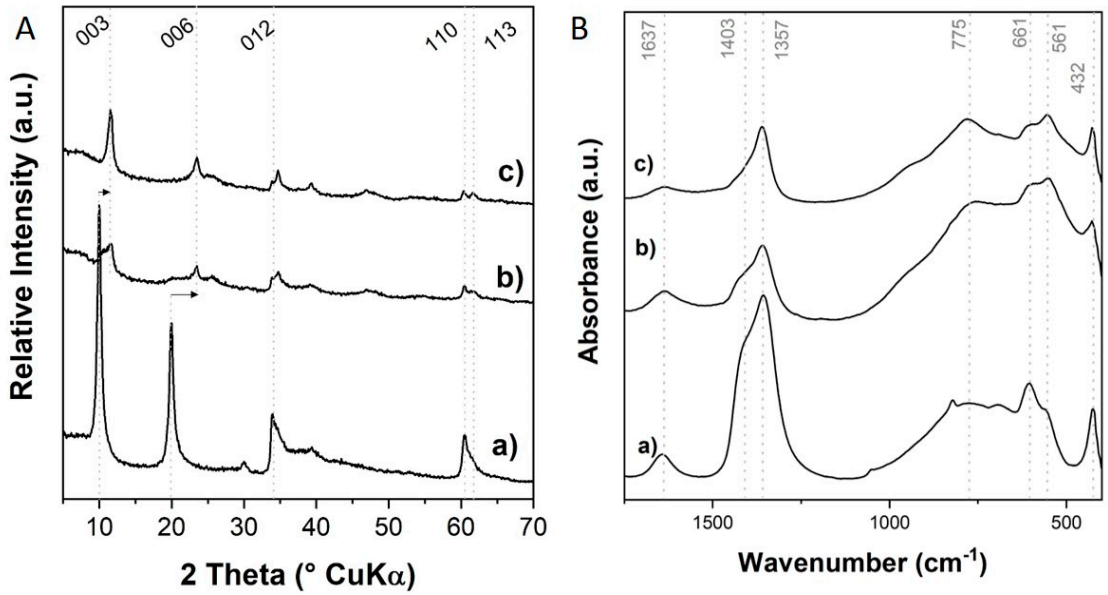

Figure 2. (**A**) PXRD patterns and (**B**) FTIR spectra of compounds obtained by impregnation method. (**a**) $[Zn_2Al\text{-}NO_3]$ precursor, (**b**) $[ZnAl/FreshTiO_2]_{2dry}$, and (**c**) $[ZnAl/FreshTiO_2]_{2wet}$.

For the $[Zn_2Al\text{-}NO_3]$ precursor, a zeta potential (ξ) of + 25 mV was measured in water, evidencing the positively charged LDH particle surface. The charge inversion of the TiO_2 surface by controlled basic titration led to a ξ value of –41 mV. These opposite ξ values are in favor of electrostatic interaction between the two components and the obtention of $[ZnAl/TiO_2]$. After a contact period of 24 h, a broadening and a decrease in the intensity of the diffraction peaks were observed, highlighting a decrease in the crystallinity of the materials. While the position of the reflection lines linked to the intralayer order was not modified, *a* shift in the 00l lines to 11.6° (0.76 nm), which corresponds to the conversion of the initial nitrate phase into a carbonate intercalated LDH, was found, despite the nitrogen atmosphere used. We assumed that the carbonate anions could come from the TiO_2 basic dispersion, since no atmosphere control was applied during the titration. Such modification of the interlayer anion was more pronounced when an undried $[Zn_2Al\text{-}NO_3]$ suspension was used, which seems to indicate that, in these conditions, anion exchange reaction is easier to carry out. *When* the dried powder of the precursors was involved in the process, only a partial anion exchange occurred, evidenced by the presence of two overlapped 003 diffraction lines around 11°, as shown in Figure 2A, and the nitrate bands at 1403 cm^{-1} which can still be observed on the FTIR spectrum, as shown in Figure 2B and in the supporting materials, Figure S3. The presence of a band at 1357 cm^{-1}, characteristic of carbonate anions, was attributed to the contamination of the matrix. However, the global decrease in the band at 1403–1357 cm^{-1} in the nanocomposites seems to indicate the replacement of nitrate and carbonate anions at the LDH particle surface. The positive surface charge compensation of the LDH layer could be mostly ensured by the negatively charged TiO_2 nanoparticles.

On the FTIR spectra, the bands related to the M-O and O-M-O bonds were unmodified after TiO_2 impregnation, which further confirmed that the LDH layer was not affected by the immobilization process. As fresh TiO_2 was used in the impregnation approach, the very small size of the colloidal TiO_2 particles, and therefore of the crystalline domains, as shown in Figure 1, induced the absence of TiO_2 characteristic reflections on the PXRD patterns, as shown in Figure 2A.

The TiO_2 immobilization on the [ZnAl] and [MgAl] matrices was next carried out by direct coprecipitation at fixed pH in the presence of TiO_2 dispersion. First, the volume of TiO_2 used was calculated to correspond to an LDH/TiO_2 ratio of 2, as previously used for the impregnation strategy. Figure 3A shows the PXRD patterns recorded for the [ZnAl] and [MgAl] LDH in using freshly prepared TiO_2. Systematically, the formation of crystallized LDH in the presence of TiO_2 was evidenced by the presence of the main diffraction lines characteristic of LDH. The [ZnAl] phase showed a particularly high crystallinity, linked to the presence of the carbonate anions in the interlayered domain, which was confirmed in particular by the interlamellar distance measured at 0.76 nm on the PXRD patterns. As for the impregnation strategy, while all of the reflection lines of the LDH matrix were present, no reflection line characteristic of TiO_2 was observed on the pattern. However, when aged TiO_2 was involved in the process for the [MgAl] matrix, in addition to the LDH reflection lines, the reflections belonging to the anatase TiO_2 were also distinguished, especially the 101 line at 25.5°, which confirmed an efficient immobilization of the TiO_2 nanoparticles within the material. Secondly, the volume of aged TiO_2 dispersion involved during the [MgAl] matrix coprecipitation was varied to prepare nanocomposites with various LDH/TiO_2 ratios, ranging from 8 to 0.66. As described above, the presence of both LDH and TiO_2 was clearly demonstrated by the observation of their characteristic diffraction lines on the patterns, as shown in Figure 3B. The relative intensities between the corresponding reflection lines of each component were strongly affected by the LDH/TiO_2 ratio. The lower ratios, which correspond to the higher TiO_2 loading, displayed, as expected, higher intensities for the TiO_2 reflection lines compared to the LDH reflection lines. On the FTIR spectra, as shown in Figure S4 and described above, all of the nanocomposites showed the LDH characteristic bands, including the ν CO_3^{2-} at 1357 cm^{-1}, which confirmed the presence of carbonate anions in the interlayer domain. The decrease in the LDH/TiO_2 ratio induced enlargement of the bands below 1000 cm^{-1} attributed to the greater contribution of the $\nu_{O\text{-}Ti\text{-}O}$ of TiO_2.

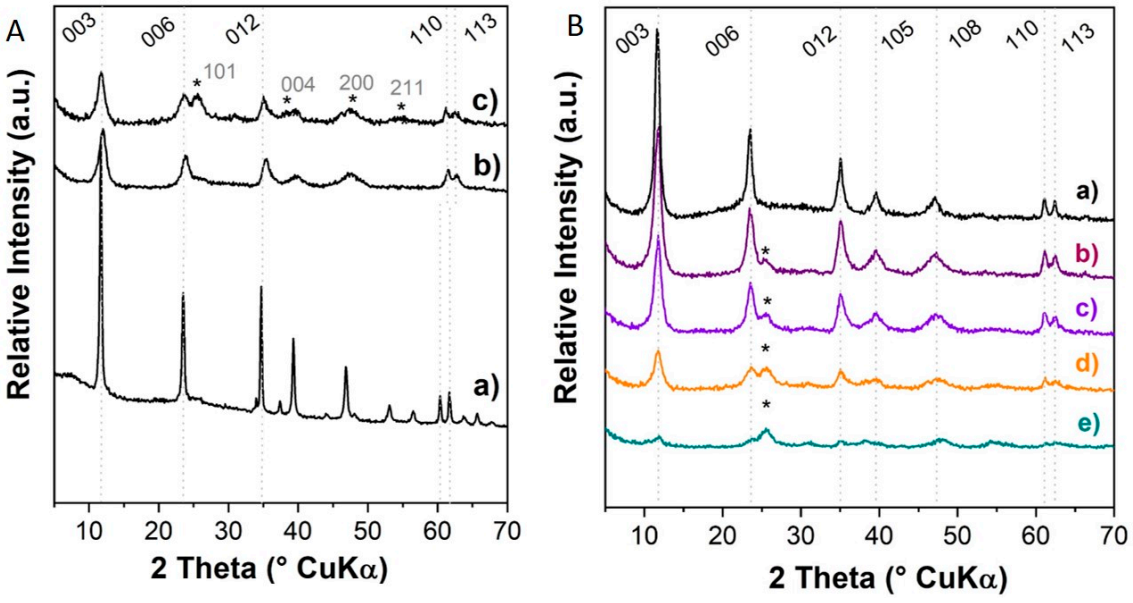

Figure 3. PXRD patterns of compounds obtained by direct coprecipitation: (**A**) with different LDH matrices and a ratio of 2 (**a**) [ZnAl/FreshTiO$_2$]$_2$, (**b**) [MgAl/FreshTiO$_2$]$_2$, and (**c**) [MgAl/AgedTiO$_2$]$_2$; (**B**) for MgAl LDH prepared with different MgAl/TiO_2 ratios (**a**) [Mg_2Al-CO_3], (**b**) [MgAl/TiO_2]$_8$, (**c**) [MgAl/TiO_2]$_4$, (**d**) [MgAl/TiO_2]$_2$, and (**e**) [MgAl/TiO_2]$_{0.66}$. * corresponds to the 101-reflection line of anatase TiO_2.

To get a better insight into the efficiency of the direct coprecipitation for immobilizing TiO_2 nanoparticles, the elementary analysis of the nanocomposites was performed, as shown in Table 1. Systematically, the LDH matrices precipitated with an Mg/Al ratio close to that theoretically fixed at 2,

whatever the amount of TiO_2 involved in the synthesis. Moreover, the higher the TiO_2 content involved in the coprecipitation, the higher the amount of TiO_2 in the nanocomposite. Compared to the TiO_2 amount involved, in all cases the percentage of TiO_2 immobilized by [MgAl] LDH was greater than 80%, even for the highest amount of TiO_2, highlighting the efficiency of the process. This value can, for instance, be advantageously compared with the one obtained in using the delamination/restacking process to immobilized TiO_2 nanoparticles, leading to an immobilization of only 53% [54].

Table 1. Main physico-chemical characteristics of the [MgAl/TiO_2] compounds prepared by coprecipitation at different ratios.

Sample	Mg/Al [a]	%TiO_2 [a]	*w*/*w* LDH/TiO_2	%TiO_2 Immobilization	nH_2O [b]	%Weight Loss	BET Surface Area (m^2 g^{-1})
[MgAl]	1.9	0	-	-	2.6	46.2	87
$[MgAl/TiO_2]_8$	1.8	8.9	10.1	81	1.5	41.6	126
$[MgAl/TiO_2]_4$	1.8	18.6	4.2	93	1.6	41.4	145
$[MgAl/TiO_2]_2$	1.9	28.0	2.7	84	2.3	40.1	190
$[MgAl/TiO_2]_{0.66}$	2.1	47.6	1.1	80	2.8	27.0	253

[a] based on ICP analysis, [b] calculated from TG analyses.

In parallel, the mole number of H_2O in each nanocomposite was determined by TGA, according to the mass loss measured between 25 °C and 125 °C, as shown in Figure 4A. The number of water molecules progressively increased in the nanocomposites when the amount of TiO_2 was higher. Oppositely, the total mass loss decreased for the lower LDH/TiO_2 ratio from 41.6% to 27.0% for a [MgAl]/TiO_2 ratio of 8 and 0.66, respectively, as shown in Table 1.

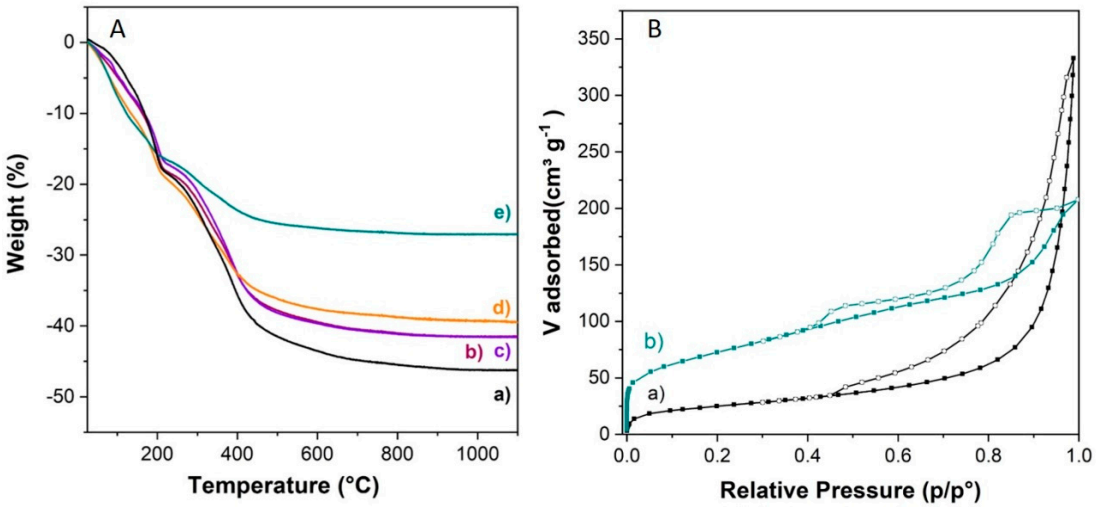

Figure 4. (**A**) TGA curves of [MgAl/TiO_2] nanocomposites obtained by coprecipitation for different MgAl/TiO_2 ratios: (**a**) [Mg_2Al-CO_3], (**b**) $[MgAl/TiO_2]_8$, (**c**) $[MgAl/TiO_2]_4$, (**d**) $[MgAl/TiO_2]_2$, and (**e**) $[MgAl/TiO_2]_{0.66}$. (**B**) N_2 adsorption-desorption isotherms of (**a**) [Mg_2Al-CO_3] and (**b**) $[MgAl/TiO_2]_{0.66}$.

Such a decrease is in good agreement with the increased amount of TiO_2 into the hydroxylated matrices, while the difference in the hydration rate into the nanocomposite may be explained by a modification of the textural properties. The surface area (Brunauer–Emmett–Teller BET) and the pore characteristics were investigated by N_2 adsorption–desorption measurements, as shown in Figure 4B and Figure S5, which clearly showed important modifications. While according to the IUPAC classification, the pure displayed a Type II adsorption isotherm with a H3 hysteresis loop, the TiO_2 immobilization into the materials progressively led to a change of the isotherm shape to a Type 4 with a H4 hysteresis.

This change of the pore shape was accompanied by a significant increase in the surface area from 126 m^2 g^{-1} to 253 m^2 g^{-1} when the [MgAl]/TiO_2 ratio fell from 8 to 0.66, emphasizing that the TiO_2

immobilization at the [MgAl] surface generated a specific interarticular porosity which could positively affect their photocatalytic performances in facilitating the accessibility of the active sites.

The morphology of the $[MgAl/TiO_2]_2$ nanocomposite obtained by coprecipitation was investigated by TEM and HRTEM as a representative sample. From the TEM image of the nanocomposite displayed in Figure 5a, it was possible to distinguish the presence of slightly darker TiO_2 nanoparticles, well dispersed on the surface of the ill-defined LDH platelets.

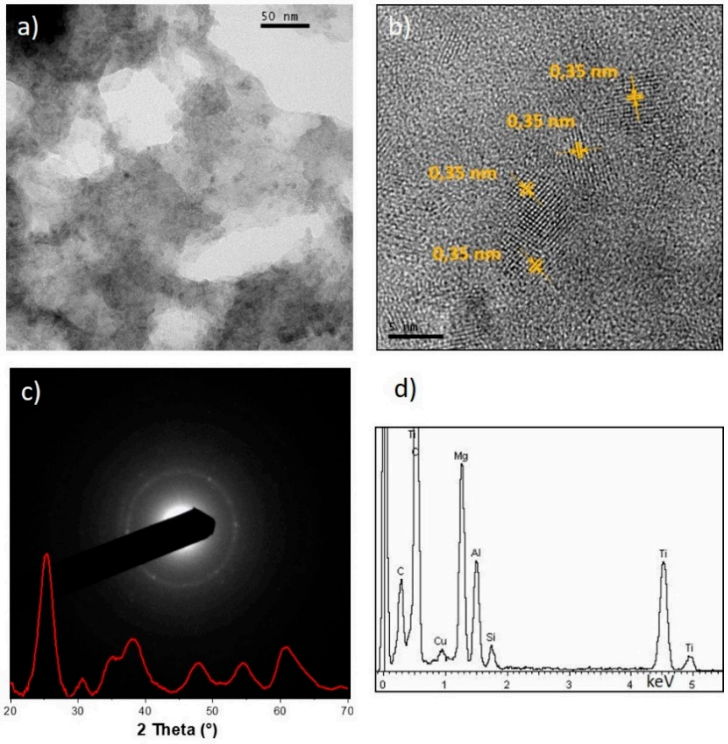

Figure 5. TEM and HRTEM analysis of the $[MgAl/TiO_2]_2$ nanocomposite obtained by coprecipitation (**a**) TEM image, (**b**) HRTEM image, (**c**) SAED pattern, and (**d**) EDX spectrum from TEM.

Note that the small size of TiO_2 particles made their observation in TEM difficult in the presence of LDH particles. The HRTEM image, shown in Figure 5b, recorded at higher magnification, further evidencing that the TiO_2 nanoparticles immobilized at the LDH surface were crystalline with a characteristic lattice spacing of 0.35 nm between the 101 planes of anatase TiO_2. In parallel, the Selected Area Electron Diffraction (SAED) also helped to gain insight into the TiO_2 crystalline structure. The red curve in Figure 5c corresponds to the average intensity over circles in the function of the scattering vector and fits well with the one expected for an anatase structure of TiO_2. EDX analyses at different selected locations, shown in Figure 5d and in the supporting materials Figure S6, confirm the results previously obtained by ICP-AES, shown in Table 1, and the local presence of the two components, LDH and TiO_2.

3.3. Photodegradation of OII in the Presence of Colloidal TiO_2 and LDH Based Nanocomposites

The immobilization of TiO_2 nanoparticles on LDH particles should facilitate the recovery of the photocatalysts from a water solution and could enhance the photocatalytic efficiency in environmental treatment processes [48]. The photocatalytic activity of colloidal TiO_2 and nanocomposites, prepared by either impregnation or coprecipitation, was evaluated by the degradation of OII ($[OII] = 5.10^{-5}$ M) at a fixed TiO_2 loading ($[TiO_2] = 0.5$ g L^{-1}) under UV-visible irradiation and compared to the efficiency of pure TiO_2 nanoparticles in basic suspensions. Blank experiments were systematically carried out in the absence of any inorganic particles (TiO_2 and LDH) and in the presence of only LDH particles (1.0 g L^{-1}), which made it possible to verify that, under our

conditions, the OII did not undergo direct hydrolysis and that the LDH had no photocatalytic effect. Figure 6A compares the degradation efficiency of pure colloidal TiO_2 in acid and basic conditions and for the fresh and aged dispersion. As previously reported [52,54], a net decrease was observed in the TiO_2 photocatalytic activity when the pH of the solution was increased. Note that acidic conditions are not compatible with environmental uses. Surprisingly, the aging of the TiO_2 dispersion, which led as described above to the enhancement of the nanoparticle crystallinity, did not strongly affect the photocatalytic behavior. Only a slight enhancement of OII degradation was noted after 2 h of irradiation.

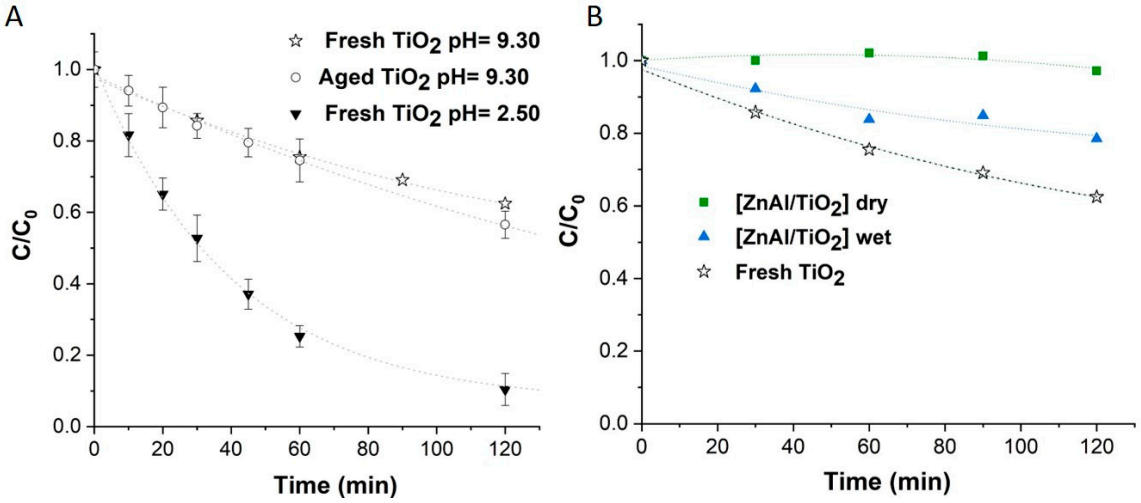

Figure 6. Variation of the concentration of OII at pH = 9.30 during photodegradation by (**A**) various colloidal TiO_2 dispersion and (**B**) [ZnAl-TiO_2] nanocomposites prepared by impregnation. Conditions: $[OII]_{initial} = 5.10^{-5}$ M; $[TiO_2] = 0.5$ g L^{-1} for all samples.

The two nanocomposites obtained by the impregnation of ZnAl LDH matrices noted that $[ZnAl/FreshTiO_2]_{2dry}$ and $[ZnAl/FreshTiO_2]_{2wet}$ were tested, as shown in Figure 6B. It should be underlined that better degradation results were obtained when the impregnation process was carried out from an undried LDH suspension compared to LDH powder, the latter displaying almost no photoactivity. These results showed that the immobilization of TiO_2 was probably more efficient using undried LDH, allowing for a greater surface interaction between the LDH and TiO_2 nanoparticles, which led to a higher immobilized amount. However, both samples displayed a reduced photocatalytic efficiency compared to pure TiO_2 basic dispersion, which could be explained by a lower quantity of photocatalyst and/or a partial aggregation and decrease in its photo efficiency.

Since impregnation did not appear as a suitable approach to immobilize TiO_2 on LDH and to produce efficient nanocomposites, we tested an alternative strategy; samples obtained by coprecipitation which corresponded to the direct formation of LDH in the presence of a dispersion of TiO_2 nanoparticles. In Figure 7A, the efficiency of the nanocomposites obtained from the chemical composition ZnAl- and MgAl-LDH and fresh TiO_2 were compared. $[MgAl/FreshTiO_2]_2$ led to the highest OII degradation. The results even further improved when aged TiO_2 was involved in the MgAl nanocomposite. In this latter case, the immobilized TiO_2 behaved at the earliest stages of the degradation in the same way as the pure colloidal aged TiO_2, while after one hour a decrease in the rate of the reaction occurred, showing a kinetic of degradation in two steps.

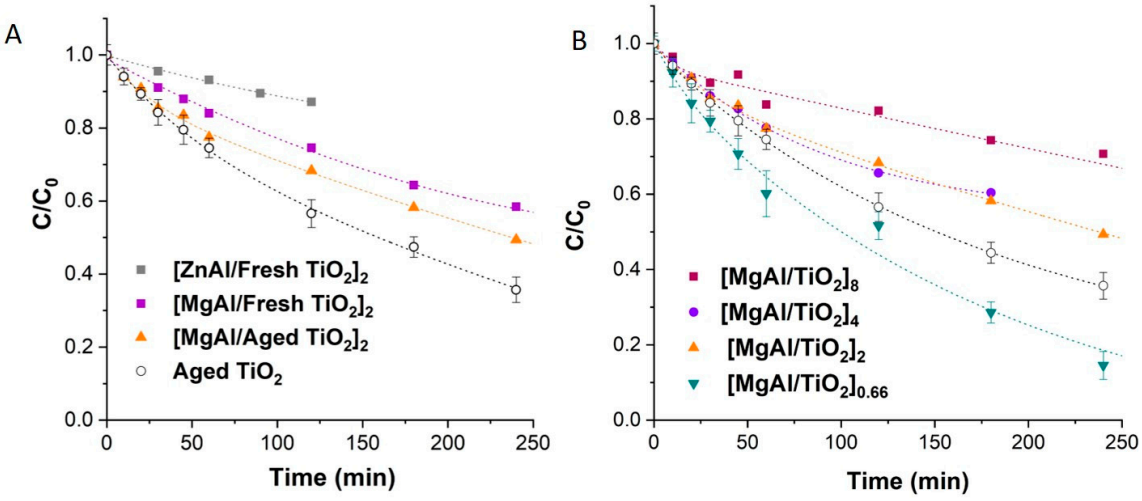

Figure 7. Variation of the concentration of OII at pH = 9.30 during photodegradation by nanocomposites prepared by direct coprecipitation (**A**) for ZnAl and MgAl LDH and fresh or aged TiO_2 and (**B**) for different MgAl/TiO_2 ratios.

To get a better insight on the photocatalytic properties of the [MgAl/TiO_2] nanocomposites obtained with aged TiO_2, a systematic study based on the amount of TiO_2 immobilized, shown in Table 1, was conducted for the different LDH/TiO_2 ratios. Since the LDH/TiO_2 experimental mass ratios were systematically higher than the theoretical ones, shown in Table 1, the amount of used nanocomposites was precisely determined to involve 0.5 g L^{-1} of TiO_2. The higher the TiO_2 amount in the nanocomposites, the greater the photodegradation of the OII, as shown in Figure 7B. Such a trend can be explained by the screening effect produced by the LDH, limiting the photon penetration in the whole suspension. Interestingly, for an experimental LDH/TiO_2 ratio of 1:1, which corresponded to the highest loading of TiO_2 within the nanocomposite tested, a faster degradation rate of OII was measured by comparison, with pure TiO_2 leading to more than 85% of degradation after 4 h of irradiation. We assumed that the homogeneous distribution of TiO_2 and the high surface area within the nanocomposite $[MgAl/TiO_2]_{0.66}$ were responsible for the enhancement of the photocatalytic properties. Under the conditions used, the photocatalytic efficiency of the optimized LDH-based nanocomposites towards OII degradation compared advantageously to those previously obtained by TiO_2 immobilized on glass slides, TiO_2/SiO_2 composites, ZnCr LDH, and derived oxides, as shown in Table S1 [55–57]. Note that the reduced graphene oxide has also been used for the immobilization of TiO_2 by a simple solvothermal method, leading to extremely efficient nanocomposites, which may be due to the ability of reduced graphene oxide to suppress the recombination of photo-induced electron-holes pairs [58].

The fate of OII in the solution and especially the complete mineralization by photodegradation using $[MgAl/TiO_2]_{0.66}$ was investigated by measuring the total organic carbon evolution in the solution, as shown in Figure 8A, B. Clearly, with increasing irradiation time, the concentration of organic carbon into the solution decreased from 13.7 mg L^{-1} to 0 after 48 h, while simultaneously the inorganic carbon content increased until 16.2 mg L^{-1}. These evolutions highlighted that the $[MgAl/TiO_2]_{0.66}$ led to the effective total mineralization of OII during the photodegradation process. These results indicate that, during the photocatalytic process, the OII is completely degraded, producing harmless byproducts such as CO_2 and H_2O. Based on the literature and our previous results [56,58], we may assume that, in the photodegradation mechanism, the HO• radical plays the main role, however, further experiments involving radical scavengers will be necessary to get a better insight into the OII degradation pathway.

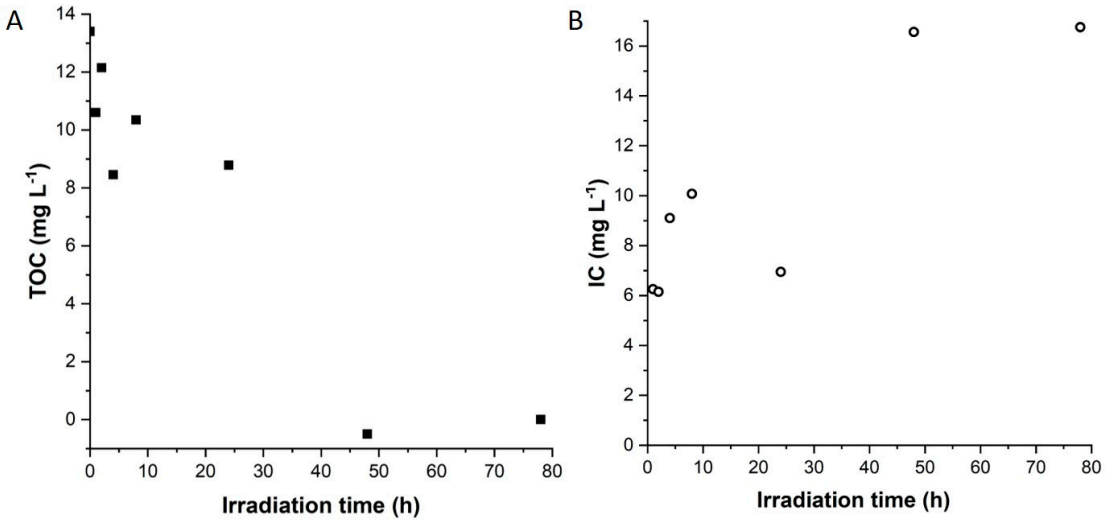

Figure 8. (**A**) Total organic carbon (TOC) and (**B**) inorganic carbon (IC) measurements under irradiation of OII in the presence of $[MgAl/TiO_2]_{0.66}$. Conditions: [OII] = 5.10^{-5} M, $[TiO_2]$ = 0.5 g L^{-1}, m$[MgAl/TiO_2]_{0.66}$ = 63.2 mg L^{-1}, pH = 9.30.

4. Conclusions

$[LDH\text{-}TiO_2]$ nanocomposites were synthesized by both impregnation and direct coprecipitation using fresh and aged TiO_2 nanoparticles. The immobilization of TiO_2 nanoparticles on the LDH surface was favored by electrostatic interactions at basic pH between negatively charged TiO_2 and positively charged LDH layers. While the $[ZnAl\text{-}TiO_2]$ nanocomposite, obtained by the impregnation of a dried LDH powder, had no photocatalytic properties, the use of the non-dried ZnAl-LDH matrix favored the immobilization of TiO_2 and led to OII photodegradation. We have shown that the coprecipitation is an efficient strategy for the immobilization of TiO_2 with a high immobilization rate (>80%). The nature of the LDH chemical composition and the aging of TiO_2 nanoparticles modified the photocatalytic efficiency of the materials, the best results being obtained by the coprecipitation of MgAl-LDH matrix and aged TiO_2. In this coprecipitation approach, the LDH/TiO_2 ratio was easily varied within the nanocomposites, which have the structural characteristics of each constituent. The presence of TiO_2 nanoparticles strongly modified the textural properties of the materials. The higher the TiO_2 loading, the greater the surface area. The best nanocomposite developed in this study was synthesized by the coprecipitation of the MgAl matrix in the presence of basic aged TiO_2 dispersion. An experimental LDH/TiO_2 ratio of 1:1 allowed us to develop a photocatalyst with more efficient than pure TiO_2 nanoparticles and it was easy to recover, leading to total OII mineralization after 48 h of irradiation. This study highlighted the importance of the method of preparing nanocomposites and the conditions used on final photocatalytic performances.

Supplementary Materials: The following are available online at http://www.mdpi.com/2305-7084/4/2/39/s1: Figure S1. UV-visible spectra of OII (5.10^{-5} M, pH = 9.30) solution in presence of $[Zn_2AlNO_3/TiO_2]_{dry}$ before and after stirring the suspension in the dark; Figure S2. FTIR spectra of $[MgAl/TiO_2]$ nanocomposite obtained by coprecipitation for different MgAl/TiO_2 ratios (a) $[Mg_2Al\text{-}CO_3]$, (b) $[MgAl/TiO_2]_8$, (c) $[MgAl/TiO_2]_4$, (d) $[MgAl/TiO_2]_2$, and (e) $[MgAl/TiO_2]_{0.66}$; Figure S3. N_2 adsorption–desorption isotherms of (a) $[MgAl/TiO_2]_8$, (b) $[MgAl/TiO_2]_4$, (c) $[MgAl/TiO_2]_2$, and (d) $[MgAl/TiO_2]_{0.66}$.

Author Contributions: Experiment, R.D.; conceptualization, G.M., V.P., and R.D.; methodology, V.P. and R.D.; validation, G.M. and V.P.; formal analysis, R.D. and V.P.; resources, R.D.; data curation, G.M. and V.P.; writing—original draft preparation, R.D. and V.P.; writing—review and editing, R.D. and V.P.; visualization, G.M.; supervision, G.M. and V.P.; project administration, V.P.; funding acquisition, R.D. All authors have read and agreed to the published version of the manuscript.

Funding: This research was funded by BOURSE D'ETUDE HORS CÔTE D'IVOIRE and CNRS France.

Acknowledgments: The organization Bourse d'Etude Hors Côte d'Ivoire is greatly acknowledged for the financial support. The authors thank Maud Clostre and Hana Mestankova for the fruitful discussion.

Conflicts of Interest: The authors declare no conflict of interest.

References

1. Oturan, M.A.; Aaron, J.-J. Advanced Oxidation Processes in Water/Wastewater Treatment: Principles and Applications. A Review. *Crit. Rev. Anal. Chem.* **2014**, *44*, 2577–2641. [CrossRef]
2. Krishnaiah, D.; Anisuzzaman, S.M.; Bono, A.; Sarbatly, R. Adsorption of 2,4,6-trichlorophenol (TCP) onto activated carbon. *J. King Saud Univ. Sci.* **2013**, *25*, 251–255. [CrossRef]
3. Sanghi, R.; Bhattacharya, B. Review on decolorisation of aqueous dye solutions by low cost adsorbents. *Coloration Technology* **2002**, *118*, 256–269. [CrossRef]
4. Kuśmierek, K. The removal of chlorophenols from aqueous solutions using activated carbon adsorption integrated with H_2O_2 oxidation. *React. Kinet. Mech. Catal.* **2016**, *119*, 19–34. [CrossRef]
5. Khorsandi, H.; Ghochlavi, N.; Aghapour, A.A. Biological Degradation of 2,4,6-Trichlorophenol by a Sequencing Batch Reactor. *Environ. Process.* **2018**, *5*, 907–917. [CrossRef]
6. Lee, J.-W.; Choi, S.-P.; Thiruvenkatachari, R.; Shim, W.-G.; Moon, H. Evaluation of the performance of adsorption and coagulation processes for the maximum removal of reactive dyes. *Dyes Pigm.* **2006**, *69*, 196–203. [CrossRef]
7. Secula, M.S.; Creţescu, I.; Petrescu, S. An experimental study of indigo carmine removal from aqueous solution by electrocoagulation. *Desalination* **2011**, *277*, 227–235. [CrossRef]
8. Beltrán-Heredia, J.; Sánchez-Martín, J.; Delgado-Regalado, A. Removal of Carmine Indigo Dye with Moringa oleifera Seed Extract. *Ind. Eng. Chem. Res.* **2009**, *48*, 6512–6520. [CrossRef]
9. Virtanen, M.T.; Hattula, M.-L. The fate of 2,4,6-trichlorophenol in an aquatic continuous-flow system. *Chemosphere* **1982**, *11*, 641–649. [CrossRef]
10. O'Neill, C.; Hawkes, F.R.; Hawkes, D.L.; Lourenço, N.D.; Pinheiro, H.M.; Delée, W. Colour in textile effluents—Sources, measurement, discharge consents and simulation: A review. *J. Chem. Technol. Biotechnol.* **1999**, *74*, 1009–1018. [CrossRef]
11. Luo, Y.; Huang, J. Hierarchical-Structured Anatase-Titania/Cellulose Composite Sheet with High Photocatalytic Performance and Antibacterial Activity. *Chem. Eur. J.* **2015**, *21*, 2568–2575. [CrossRef]
12. Li, Y.; Wang, P.; Huang, C.; Yao, W.; Wu, Q.; Xu, Q. Synthesis and photocatalytic activity of ultrafine Ag3PO4 nanoparticles on oxygen vacated TiO_2. *Appl. Catal., B* **2017**, *205*, 489–497. [CrossRef]
13. Gutiérrez-Segura, E.; Solache-Ríos, M.; Colín-Cruz, A. Sorption of indigo carmine by a Fe-zeolitic tuff and carbonaceous material from pyrolyzed sewage sludge. *J. Hazard. Mater.* **2009**, *170*, 1227–1235. [CrossRef] [PubMed]
14. Kanan, S.; Moyet, M.A.; Arthur, R.B.; Patterson, H.H. Recent advances on TiO_2-based photocatalysts toward the degradation of pesticides and major organic pollutants from water bodies. *Catal. Rev.* **2020**, *62*, 1–65. [CrossRef]
15. Guo, Q.; Zhou, C.; Ma, Z.; Yang, X. Fundamentals of TiO_2 Photocatalysis: Concepts, Mechanisms, and Challenges. *Adv. Mater.* **2019**, *31*, 1901997. [CrossRef] [PubMed]
16. Parfitt, G.D. The Surface of Titanium Dioxide. In *Progress in Surface and Membrane Science*; Cadenhead, D.A., Danielli, J.F., Eds.; Elsevier: Amsterdam, The Netherlands, 1976; Volume 11, pp. 181–226.
17. Augustynski, J. Aspects of photo-electrochemical and surface behaviour of titanium (IV) oxide. In *Solid Materials*; Springer: Berlin/Heidelberg, Germany, 1988; pp. 1–61.
18. Ohtani, B.; Nishimoto, S. Effect of surface adsorptions of aliphatic alcohols and silver ion on the photocatalytic activity of titania suspended in aqueous solutions. *J. Phys. Chem.* **1993**, *97*, 920–926. [CrossRef]
19. Mihaylov, B.V.; Hendrix, J.L.; Nelson, J.H. Comparative catalytic activity of selected metal oxides and sulfides for the photo-oxidation of cyanide. *J. Photochem. Photobiol. A* **1993**, *72*, 173–177. [CrossRef]
20. Karakitsou, K.E.; Verykios, X.E. Effects of altervalent cation doping of titania on its performance as a photocatalyst for water cleavage. *J. Phys. Chem.* **1993**, *97*, 1184–1189. [CrossRef]
21. Goel, M.; Chovelon, J.-M.; Ferronato, C.; Bayard, R.; Sreekrishnan, T.R. The remediation of wastewater containing 4-chlorophenol using integrated photocatalytic and biological treatment. *J. Photochem. Photobiol. B* **2010**, *98*, 1–6. [CrossRef] [PubMed]

22. Garcia-Segura, S.; Brillas, E. Applied photoelectrocatalysis on the degradation of organic pollutants in wastewaters. *J. Photochem. Photobiol. C* **2017**, *31*, 1–35. [CrossRef]
23. Qian, R.; Zong, H.; Schneider, J.; Zhou, G.; Zhao, T.; Li, Y.; Yang, J.; Bahnemann, D.W.; Pan, J.H. Charge carrier trapping, recombination and transfer during TiO_2 photocatalysis: An overview. *Catal. Today* **2019**, *335*, 78–90. [CrossRef]
24. Nam, Y.; Lim, J.H.; Ko, K.C.; Lee, J.Y. Photocatalytic activity of TiO_2 nanoparticles: A theoretical aspect. *J. Mater. Chem. A* **2019**, *7*, 13833–13859. [CrossRef]
25. Behnajady, M.A.; Modirshahla, N.; Mirzamohammady, M.; Vahid, B.; Behnajady, B. Increasing photoactivity of titanium dioxide immobilized on glass plate with optimization of heat attachment method parameters. *J. Hazard. Mater.* **2008**, *160*, 508–513. [CrossRef] [PubMed]
26. Khataee, A.R.; Pons, M.N.; Zahraa, O. Photocatalytic degradation of three azo dyes using immobilized TiO2 nanoparticles on glass plates activated by UV light irradiation: Influence of dye molecular structure. *J. Hazard. Mater.* **2009**, *168*, 451–457. [CrossRef] [PubMed]
27. Papoutsi, D.; Lianos, P.; Yianoulis, P.; Koutsoukos, P. Sol-Gel Derived TiO_2 Microemulsion Gels and Coatings. *Langmuir* **1994**, *10*, 1684–1689. [CrossRef]
28. Zhang, S.; Zhu, Y.F.; Brodie, D.E. Photoconducting TiO_2 prepared by spray pyrolysis using $TiCl_4$. *Thin Solid Films* **1992**, *213*, 265–270. [CrossRef]
29. Mamaghani, A.H.; Haghighat, F.; Lee, C.-S. Hydrothermal/solvothermal synthesis and treatment of TiO_2 for photocatalytic degradation of air pollutants: Preparation, characterization, properties, and performance. *Chemosphere* **2019**, *219*, 804–825. [CrossRef] [PubMed]
30. Carreon, M.A.; Choi, S.Y.; Mamak, M.; Chopra, N.; Ozin, G.A. Pore architecture affects photocatalytic activity of periodic mesoporous nanocrystalline anatase thin films. *J. Mater. Chem.* **2007**, *17*, 82–89. [CrossRef]
31. Carreon, M.L.; Carreon, H.G.; Espino-Valencia, J.; Carreon, M.A. Photocatalytic degradation of organic dyes by mesoporous nanocrystalline anatase. *Mater. Chem. Phys.* **2011**, *125*, 474–478. [CrossRef]
32. Katti, A.; Venna, S.R.; Carreon, M.A. Self-assembly hydrothermal assisted synthesis of mesoporous anatase in the presence of ethylene glycol. *Catal. Commun.* **2009**, *10*, 2036–2040. [CrossRef]
33. Khammar, S.; Bahramifar, N.; Younesi, H. Preparation and surface engineering of CM-β-CD functionalized Fe_3O_4@TiO_2 nanoparticles for photocatalytic degradation of polychlorinated biphenyls (PCBs) from transformer oil. *J. Hazard. Mater.* **2020**, *394*, 122422. [CrossRef] [PubMed]
34. Forano, C.; Costantino, U.; Prévot, V.; Gueho, C.T. Chapter 14.1—Layered Double Hydroxides (LDH). In *Developments in Clay Science*; Bergaya, F., Lagaly, G., Eds.; Elsevier: Amsterdam, The Netherlands, 2013; Volume 5, pp. 745–782.
35. Rives, V. (Ed.) *Layered Double Hydroxides: Present and Future*; Nova Science Publishers, Inc.: New York, NY, USA, 2001; p. 439.
36. Chubar, N.; Gilmour, R.; Gerda, V.; Micusik, M.; Omastova, M.; Heister, K.; Man, P.; Fraissard, J.; Zaitsev, V. Layered double hydroxides as the next generation inorganic anion exchangers: Synthetic methods versus applicability. *Adv. Colloid Interface Sci.* **2017**, *245*, 62–80. [CrossRef] [PubMed]
37. Lu, Y.; Jiang, B.; Fang, L.; Ling, F.; Gao, J.; Wu, F.; Zhang, X. High performance NiFe layered double hydroxide for methyl orange dye and Cr(VI) adsorption. *Chemosphere* **2016**, *152*, 415–422. [CrossRef] [PubMed]
38. Grégoire, B.; Bantignies, J.-L.; Le-Parc, R.; Prélot, B.; Zajac, J.; Layrac, G.; Tichit, D.; Martin-Gassin, G. Multiscale Mechanistic Study of the Adsorption of Methyl Orange on the External Surface of Layered Double Hydroxide. *J. Phys. Chem. C* **2019**, *123*, 22212–22220. [CrossRef]
39. Bouhent, M.; Derriche, Z.; Denoyel, R.; Prevot, V.; Forano, C. Thermodynamical and structural insights of orange II adsorption by Mg_RAlNO_3 layered double hydroxides. *J. Solid State Chem.* **2011**, *184*, 1016–1024. [CrossRef]
40. Chivu, V.; Gilea, D.; Cioatera, N.; Carja, G.; Mureseanu, M. Heterostructures of Ce-Ti/layered double hydroxides and the derived MMOs for photoenergy applications. *Appl. Surf. Sci.* **2020**, *513*, 145853. [CrossRef]
41. Egambaram, O.P.; Pillai, S.K.; Lategan, M.; Ray, S.S. Nanostructured Zn-Ti layered double hydroxides with reduced photocatalytic activity for sunscreen application. *J. Nanopart. Res.* **2019**, *21*, 1–12. [CrossRef]
42. Liu, X.; Chen, Z.; Cao, M. NiFe Layered Double Hydroxide on Nitrogen Doped TiO_2 Nanotube Arrays toward Efficient Oxygen Evolution. *ACS Appl. Energy Mater.* **2019**, *2*, 5960–5967. [CrossRef]

43. Pourradi, H.; Ghani, K.; Mahdavi, M. Advanced Interface Engineering of $CH_3NH_3PbI_3$ Perovskite Solar Cells: The Unique Role of Layered Double Hydroxide Precursor. *ACS Appl. Energy Mater.* **2020**, *3*, 1476–1483. [CrossRef]
44. Ran, L.; Yin, L. Ternary Hierarchical Cu_7S_4/TiO_2/CoCr-LDH Heterostructured Nanorod Arrays with Multiphase Reaction Interfaces for More Efficient Photoelectrochemical Water Splitting. *Adv. Mater. Interfaces* **2019**, *6*, 1–14. [CrossRef]
45. Vucetic, S.B.; Rudic, O.L.; Markov, S.L.; Bera, O.J.; Vidakovic, A.M.; Skapin, A.S.S.; Ranogajec, J.G. Antifungal efficiency assessment of the TiO2 coating on facade paints. *Environ. Sci. Pollut. Res.* **2014**, *21*, 11228–11237. [CrossRef] [PubMed]
46. Zhang, G.; Zhang, X.; Meng, Y.; Pan, G.; Ni, Z.; Xia, S. Layered double hydroxides-based photocatalysts and visible-light driven photodegradation of organic pollutants: A review. *Chem. Eng. J. (Amsterdam Neth.)* **2020**, *392*, 123684. [CrossRef]
47. Zhu, H.; Liu, Q.; Li, Z.; Liu, J.; Jing, X.; Zhang, H.; Wang, J. Synthesis of exfoliated titanium dioxide nanosheets/nickel-aluminum layered double hydroxide as a novel electrode for supercapacitors. *RSC Adv.* **2015**, *5*, 49204–49210. [CrossRef]
48. Ziarati, A.; Badiei, A.; Grillo, R.; Burgi, T. 3D Yolk@Shell TiO_2-x/LDH Architecture: Tailored Structure for Visible Light CO2 Conversion. *ACS Appl. Mater. Interfaces* **2019**, *11*, 5903–5910. [CrossRef] [PubMed]
49. Kun, R.; Balazs, M.; Dekany, I. Photooxidation of organic dye molecules on TiO_2 and zinc-aluminum layered double hydroxide ultrathin multilayers. *Colloids Surf. A* **2005**, *265*, 155–162. [CrossRef]
50. Mourid, E.H.; El Mouchtari, E.M.; El Mersly, L.; Benaziz, L.; Rafqah, S.; Lakraimi, M. Development of a new recyclable nanocomoposite LDH-TiO_2 for the degradation of antibiotic sulfamethoxazole under UVA radiation: An approach towards sunlight. *J. Photochem. Photobiol. A* **2020**, *396*, 112530. [CrossRef]
51. Seftel, E.M.; Niarchos, M.; Vordos, N.; Nolan, J.W.; Mertens, M.; Mitropoulos, A.C.; Vansant, E.F.; Cool, P. LDH and TiO_2/LDH-type nanocomposite systems: A systematic study on structural characteristics. *Microporous Mesoporous Mater.* **2015**, *203*, 208–215. [CrossRef]
52. Paušová, Š.; Krýsa, J.; Jirkovský, J.; Forano, C.; Prevot, V.; Mailhot, G. Photocatalytic properties of aqueous systems containing TiO_2 nanoparticles. *Catal. Today* **2011**, *161*, 140–146. [CrossRef]
53. Kormann, C.; Bahnemann, D.W.; Hoffmann, M.R. Photolysis of chloroform and other organic molecules in aqueous titanium dioxide suspensions. *Environ. Sci. Technol.* **1991**, *25*, 494–500. [CrossRef]
54. Pausova, S.; Krysa, J.; Jirkovsky, J.; Mailhot, G.; Prevot, V. Photocatalytic behavior of nanosized TiO_2 immobilized on layered double hydroxides by delamination/restacking process. *Environ. Sci. Pollut. Res.* **2012**, *19*, 3709–3718. [CrossRef] [PubMed]
55. Onam Onyatta, J.; Kimutai Tum, P.; Kithure, J.G.N.; Oduor, F.D.O. Photocatalytic degradation of acid Orange II dye on selected commercial titanium dioxide catalysts. *Int. J. Adv. Res.* **2016**, *4*, 1149–1155.
56. Paušová, Š.; Krýsa, J.; Jirkovský, J.; Forano, C.; Mailhot, G.; Prevot, V. Insight into the photocatalytic activity of ZnCr–CO_3 LDH and derived mixed oxides. *Appl. Catal. B* **2015**, *170–171*, 25–33. [CrossRef]
57. Paušová, Š.; Krýsa, J.; Jirkovský, J.; Prevot, V.; Mailhot, G. Preparation of TiO_2-SiO_2 composite photocatalysts for environmental applications. *J. Chem. Technol. Biotechnol.* **2014**, *89*, 1129–1135. [CrossRef]
58. Li, T.; Wang, T.; Qu, G.; Liang, D.; Hu, S. Synthesis and photocatalytic performance of reduced graphene oxide–TiO_2 nanocomposites for orange II degradation under UV light irradiation. *Environ. Sci. Pollut. Res.* **2017**, *24*, 12416–12425. [CrossRef] [PubMed]